


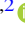



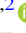




An Extraordinary Response of Iron Emission to the Central Outburst in a Tidal Disruption Event Candidate

Zhicheng He^{1,2} , Ning Jiang^{1,2} , Tinggui Wang^{1,2} , Guilin Liu^{1,2} , Mouyuan Sun³ , Hengxiao Guo⁴ , Lu Shen^{1,2},
Zhenyi Cai^{1,2}, Xinwen Shu⁵ , Zhenfeng Sheng^{1,2}, Zhixiong Liang^{1,2} , and Youhua Xu⁶

¹ Key laboratory for Research in Galaxies and Cosmology, Department of Astronomy, University of Science and Technology of China, Chinese Academy of Sciences, Hefei, Anhui 230026, People's Republic of China; zcho@ustc.edu.cn, jnac@ustc.edu.cn, twang@ustc.edu.cn

² School of Astronomy and Space Sciences, University of Science and Technology of China, Hefei, Anhui 230026, People's Republic of China

³ Department of Astronomy, Xiamen University, Xiamen, Fujian 361005, People's Republic of China

⁴ Department of Physics and Astronomy, 4129 Frederick Reines Hall, University of California, Irvine, CA, 92697-4575, USA

⁵ Department of Physics, Anhui Normal University, Wuhu, Anhui, 241000, People's Republic of China

⁶ CAS Key Laboratory of Space Astronomy and Technology, National Astronomical Observatories, Beijing, People's Republic of China

Received 2020 December 18; revised 2021 January 3; accepted 2021 January 4; published 2021 January 28

Abstract

Understanding the origin of Fe II emission is important because it is crucial to construct the main sequence of active galactic nuclei (AGNs). Despite several decades of observational and theoretical effort, the location of the optical iron emitting region and the mechanism responsible for the positive correlation between the Fe II strength and the black hole accretion rate remain open questions. In this Letter, we report the optical Fe II response to the central outburst in PS1-10adi, a candidate tidal disruption event taking place in an AGN at $z = 0.203$ that has aroused extensive attention. For the first time, we observe that the Fe II response in the rising phase of its central luminosity is significantly more prominent than that in the decline phase, showing a hysteresis effect. We interpret this hysteresis effect as a consequence of the gradual sublimation of the dust grains situating at the inner surface of the torus into gas when the luminosity of the central engine increases. It is the iron element released from the sublimated dust that contributes evidently to the observed Fe II emission. This interpretation, together with the weak response of the $H\beta$ emission as we observe, naturally explains the applicability of relative Fe II strength as a tracer of the Eddington ratio. In addition, optical iron emission of this origin renders the Fe II time lag a potential “standard candle” with cosmological implications.

Unified Astronomy Thesaurus concepts: [Tidal disruption \(1696\)](#); [Time domain astronomy \(2109\)](#); [Standard candles \(1563\)](#); [Active galactic nuclei \(16\)](#)

1. Introduction

An active galactic nucleus (AGN) powered by the super-massive black hole (BH) accretion disk is the most luminous persistent celestial object in the universe, and can be observed up to $z > 7$ (Mortlock et al. 2011; Bañados et al. 2018; Yang et al. 2020). Some features of AGN have the potentiality to establish as standard candles, such as the broad line region (BLR) size and luminosity relation (Watson et al. 2011; Czerny et al. 2013; Wang et al. 2020) and the nonlinear relation between UV and X-ray luminosities (Risaliti & Lusso 2019) or flux variability (Sun et al. 2018). The reliability of an AGN as a standard candle depends on our understanding of AGN structure and the related physical process. Blends of Fe II emission lines are a prominent feature in the ultraviolet (UV) and optical spectra of AGNs. The relative strength of optical iron, is one of the major characteristics of “Eigenvector 1” driven by the most important quantity of the BH accretion system, the Eddington ratio (Boroson & Green 1992; Boroson 2002; Shen & Ho 2014). Despite several decades of observational and theoretical effort (Boroson & Green 1992; Wang et al. 1996; Lawrence et al. 1997; Marziani et al. 2001; Boroson 2002; Ferland et al. 2009; Shields et al. 2010; Dong et al. 2011; Shen & Ho 2014; Panda et al. 2018, 2019), the physical mechanism of Fe II emissions has remained very difficult to determine. Studying the origin of Fe II can promote our understanding of AGN structure and the related physical processes, hence improving the reliability of AGN as a standard candle.

Recent progress in the time domain surveys has led to numerous discoveries of outburst events in AGN (e.g., Kankare et al. 2017; Trakhtenbrot et al. 2019). Among them, tidal disruption events (TDEs) include a star that is occasionally ripped apart by the tidal force of SMBHs (Rees 1988). TDEs in AGNs are of particular interest in that they offer us a unique opportunity to revisit, in a dynamic way, open questions about AGN structure and the related physics process on a timescale of months to years. For example, the luminous infrared emission of AGN TDEs, originating from the dust reprocessed emission, can yield valuable information on the dusty torus (Jiang et al. 2019). The other fascinating characteristic associated with those TDE events is the dramatic increase of the Fe II emission after the outburst; though, they will fade away later on (e.g., Drake et al. 2011; Blanchard et al. 2017; Kankare et al. 2017). The transient Fe II emission has been proposed as a natural result of sublimation of dust grains located in the inner torus due to the sharp increasing of the central emission (Jiang et al. 2017, 2019). The iron elements primarily locked in the dust phase are released and transferred into the gas phase, contributing significantly to the Fe II emission. However, this assumption lacks convincing evidence.

In this work, we carry out a detailed analysis of the well-known TDE candidate in PS1-10adi (an AGN at $z = 0.203$) to study the physical process of optical Fe II emission and its potential cosmological applications. The paper is organized as follows. In Section 2, we present the data and spectral fitting. In Section 3, we analyze the emission region of optical Fe II in

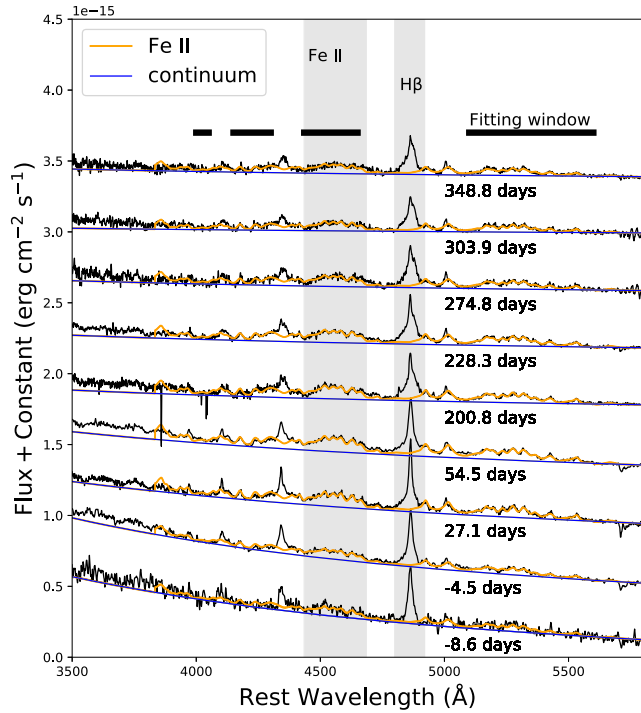


Figure 1. The spectral data of PS1-10adi (from the supplementary Figure 2 of Kankare et al. 2017). A power law plus the optical Fe II template (Boroson & Green 1992) to fit the continuum and Fe II emission. The black horizontal lines mark the fitting regions that are relatively free from strong emission lines except Fe II. The gray shadow regions mark the locations of Fe II 4435–4685 Å and H β .

TDE. In Section 4, we present the discussions. Throughout this work, we adopt a standard Λ CDM cosmology with $H_0 = 70 \text{ km s}^{-1} \text{ Mpc}^{-1}$, $\Omega_m = 0.3$, and $\Omega_\Lambda = 0.7$.

2. Data and Spectral Fitting

PS1-10adi was initially discovered by the Panoramic Survey Telescope and Rapid Response System (Pan-STARRS) and was suggested as an energetic TDE candidate in AGN at $z = 0.203$ (Kankare et al. 2017; Jiang et al. 2019). It stands out from AGN flares reported in the past few years because of the comprehensive observing campaign performed since its discovery, particularly its massive optical spectral data, which has rarely covered the stage prior to the luminosity peak. The follow-up spectra taken at different stages (see Figure 1) give us an excellent data set to explore how the Fe II strength and relative Fe II strength, i.e., $R_{\text{Fe II}} = f_{\text{Fe II}}/f_{\text{H}\beta}$, respond to the large amplitude of variation in the accretion rate. The $f_{\text{Fe II}}$ is calculated in the range of 4435–4685 Å (the left gray shaded region in Figure 1).

As shown in Figure 1, we adopt a power law $f_\lambda \propto \lambda^{-\alpha}$ plus the optical Fe II template (Boroson & Green 1992) to fit the continuum and Fe II emission in the wavelength regions: 4000–4050 Å, 4150–4300 Å, 4435–4650 Å, 5100–5600 Å, which are relatively free from the strong emission lines except Fe II. We repeat this fitting process 1000 times. For each time, we add a Gaussian random error to the observed flux. The flux of H β are the observed flux by subtracting Fe II emission and continuum: $f_{\text{H}\beta} = f_{\text{obs}} - f_{\text{Fe II}} - f_{\text{con}}$. The best-fitted results and the corresponding errors are the mean and standard deviation from the 1000 fittings, respectively. The spectral data and fitting results are shown in Table 1.

3. The Emission Region of Optical Fe II in PS1-10adi

3.1. The Time Lag of Fe II Relative to the Continuum

From Figure 2, it can be easily seen that the Fe II emission and $R_{\text{Fe II}}$ rise rapidly and reach the maximum after 55 days of the optical photometry luminosity ($L_{\text{uv-optical}}$, hereafter L) peak, and then decline gradually. Meanwhile, the H β emission also has a weak response to the change of central radiation. We notice a gap of Fe II observations between day 55 and day 200. Thus, the real Fe II peak might occur later than 55 days. A theoretical calculation (Namekata & Umemura 2016) of dust sublimation radius is as follows:

$$R_{\text{sub}} = 0.121 \text{ pc} \left(\frac{L_{\text{bol}}}{10^{45} \text{ erg s}^{-1}} \right)^{0.5} \left(\frac{T_{\text{sub}}}{1800 \text{ K}} \right)^{-2.8} \times \left(\frac{a}{0.1 \mu\text{m}} \right)^{-0.5}, \quad (1)$$

where T_{sub} is the sublimation temperature of dust, and a is the radius of the dust grain. Given the peak luminosity $L = 5 \times 10^{44} \text{ erg s}^{-1}$, the theoretical torus inner radius R_{sub} is about 0.085 pc, corresponding to 100 light days. Kishimoto et al. (2007) found that the innermost torus radii based on dust reverberation were systematically smaller than the theoretical prediction of Equation (1) by a factor of ~ 3 . Thus, the observed time lag is roughly consistent with the torus inner radius. Nevertheless, the observed time lag is not enough to prove that the Fe II radiation is related to the torus inner radius. In the following two subsections, we will analyze the Fe II emission region by its evolutionary trajectory.

3.2. The Hysteresis Phenomenon of the Fe II Evolutionary Trajectory

As shown in Figure 2, to analyze the emission region of optical Fe II, we shift the photometry data for 55 days to align the peaks of Fe II emission and L . The green stars in panel (a) of Figure 2 are the interpolation luminosities at the corresponding time of spectral observations.

We adopt the power-law function to analyze the line emission response to the change of central radiation: $\log_{10} f_{\text{line}} = \alpha \log_{10} L + \beta$, where α is the power-law slope and β is the intercept. As shown in panel (a) of Figure 3, the best-fitted α is 0.63 ± 0.04 and 0.27 ± 0.02 for Fe II in the luminosity rising (before peak) and decline (after peak) phases, respectively. Interestingly, the Fe II variation rate (described by the slope α) in the luminosity rising phase is significantly greater than that in the decline phase. At the same luminosity, the Fe II strength in the decline phase is significantly larger than that in the rising phase. The evolutionary trajectory of Fe II forms a “ Λ ” shape (i.e., a hysteresis effect), which indicates that the amount of Fe II-emitting gas in the decline phase is larger than that in the rising phase. Even if we shift the photometry data for 100 days (corresponding to the theoretical torus inner radius), the hysteresis effect of the Fe II evolutionary trajectory will still exist.

Note that we did not take into account the systematic uncertainties of the spectral flux calibrations in the above analysis. As a result, the absolute flux of Fe II or H β lines may not be so credible. However, the $R_{\text{Fe II}}$, i.e., relative Fe II strength is less affected by the systematic uncertainties of the flux calibrations. The evolutionary trajectory of $R_{\text{Fe II}}$ is shown in panel (b) of Figure 3.

Table 1
The Spectral Data and Fitting Result for Fe II and H β Lines

Time Relative to Peak (days)	$\log L$ (ergs $^{-1}$)	Fe II ($\times 10^{-14}$ erg cm $^{-2}$ s $^{-1}$)	H β ($\times 10^{-14}$ erg cm $^{-2}$ s $^{-1}$)	$R_{\text{Fe II}}$
-8.6	44.36	1.101 \pm 0.030	0.997 \pm 0.004	1.10 \pm 0.03
-4.5	44.38	1.167 \pm 0.012	1.097 \pm 0.002	1.06 \pm 0.01
27.1	44.56	1.665 \pm 0.015	1.205 \pm 0.003	1.38 \pm 0.01
54.5	44.71	1.888 \pm 0.011	1.218 \pm 0.002	1.55 \pm 0.01
200.8	44.34	1.604 \pm 0.012	1.113 \pm 0.002	1.44 \pm 0.01
228.3	44.27	1.573 \pm 0.011	1.129 \pm 0.002	1.39 \pm 0.01
274.8	44.16	1.362 \pm 0.052	1.038 \pm 0.006	1.31 \pm 0.04
303.9	44.10	1.135 \pm 0.013	0.860 \pm 0.002	1.32 \pm 0.01
348.8	44.00	1.195 \pm 0.039	0.946 \pm 0.005	1.26 \pm 0.03

Note. The luminosity corresponding to each spectrum is the result of interpolation in the optical photometry luminosity (green stars in Figure 2).

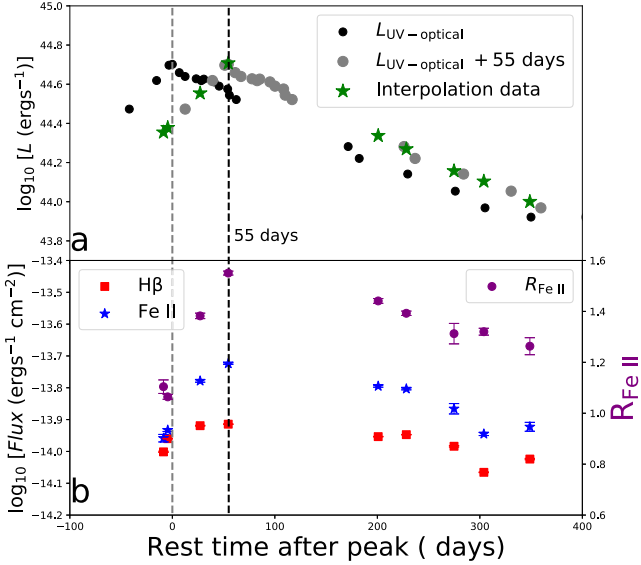


Figure 2. The UV–optical luminosity and line flux evolution of PS1-10adi. Panel (a): the black points are the UV–optical photometry luminosity. The gray points are the luminosity shifted by 55 days to align with the peak of Fe II emission. The green stars are the interpolation data at the corresponding time of spectral observations. Panel (b): the red squares, blue stars, and purple points represent the H β , Fe II, and $R_{\text{Fe II}}$, respectively. The Fe II and $R_{\text{Fe II}}$ rise rapidly and reach the maximum after 55 days of the luminosity peak, and then decline gradually.

The best-fitted α are 0.47 ± 0.01 and 0.11 ± 0.01 for $R_{\text{Fe II}}$ in the central luminosity rising and decline phases, respectively. The “A” shape may be the reason for the scattered correlation between Fe II strength and accretion rate, especially at the low accretion rate state (see right panels of Figure 10 in Dong et al. 2011). If we divide a sample into two parts: the luminosity rising and declining phases, the correlation between Fe II strength and accretion rate of the luminosity rising phase should be stronger than that of the whole sample.

3.3. Fe II Emission Dominated by the Evaporated Dust at the inner Radius of the Torus

As shown in Figure 4, we propose a scenario to interpret the physical process of the Fe II hysteresis effect. As the central luminosity increases, the dust at the torus’ inner radius gradually sublimates into gas. The metals released from the evaporated dust will boost the observed Fe II line. The amount of evaporated dust reaches the maximum at the peak of central

luminosity. The observations of NGC4151 (Koshida et al. 2009; Kishimoto et al. 2013) and Mrk 590 (Kokubo & Minezaki 2020) suggest the dust condensation/reformation timescale is around a few years. Thus, the amount of evaporated dust will remain the maximum for at least a few months after the peak of central luminosity. At the same luminosity, the Fe II emission in the decline phase will be greater than that in the rising phase. Meanwhile, the best-fitted α are 0.15 ± 0.04 and 0.16 ± 0.02 for H β in the luminosity rising and declining phases, respectively. There is no significant difference for H β variation rate between these two phases. This result indicates that the H β emitter region is smaller than the torus’ inner radius and H β is not dominated by the evaporated dust, but by the BLR gas.

The intriguing hysteresis effect of Fe II or $R_{\text{Fe II}}$ evolutionary trajectory strongly suggests that the increased Fe II emission is linked to the evaporated dust at a scale of torus inner radius. In this scenario, the Fe II strength is mainly regulated by the amount of gas-phase iron (see also Shields et al. 2010). As the central luminosity increases, the inner boundary of the dusty torus will recede to a larger radius. During this process, the irons released from the sublimated dust contribute evidently to the Fe II emission. Meanwhile, the weak response of H β also implies that its dominant radiation region is likely closer than that of Fe II, which is consistent with the reverberation mapping results (e.g., Barth et al. 2013). When the central luminosity increases, the response of Fe II is stronger than that of H β resulting in the increasing of the relative Fe II strength $R_{\text{Fe II}}$. As a result, the relative Fe II strength has been observed as an indicator of the Eddington ratio of AGNs.

4. Discussions

4.1. A Potential Cosmological Standard Candle Based on Fe II

Our results suggest that the Fe II emission is boosted by the new evaporated dust at the inner radius of the torus in TDE. In view of this, the time lag between the optical continuum peak and optical Fe II peak can be adopted as “standard candles” in cosmology. The AGN luminosity L_{bol} and the dust sublimation radius R_{sub} can be written as (Hoenig & Kishimoto 2011; Hönig et al. 2017):

$$L_{\text{bol}} = 16\pi R_{\text{sub}}^2 f_{\text{abs}}^{-1} Q_{\text{abs}}; p(T_{\text{sub}}) \sigma_{\text{SB}} T_{\text{sub}}^4, \quad (2)$$

where f_{abs} is the fraction of incident AGN flux absorbed per dust particle and $Q_{\text{abs}}; p(T_{\text{sub}})$ is the normalized Planck-mean absorption efficiency of the dust. Note that f_{abs} and $Q_{\text{abs}}; p$ are related with both parameters approaching unity for large dust

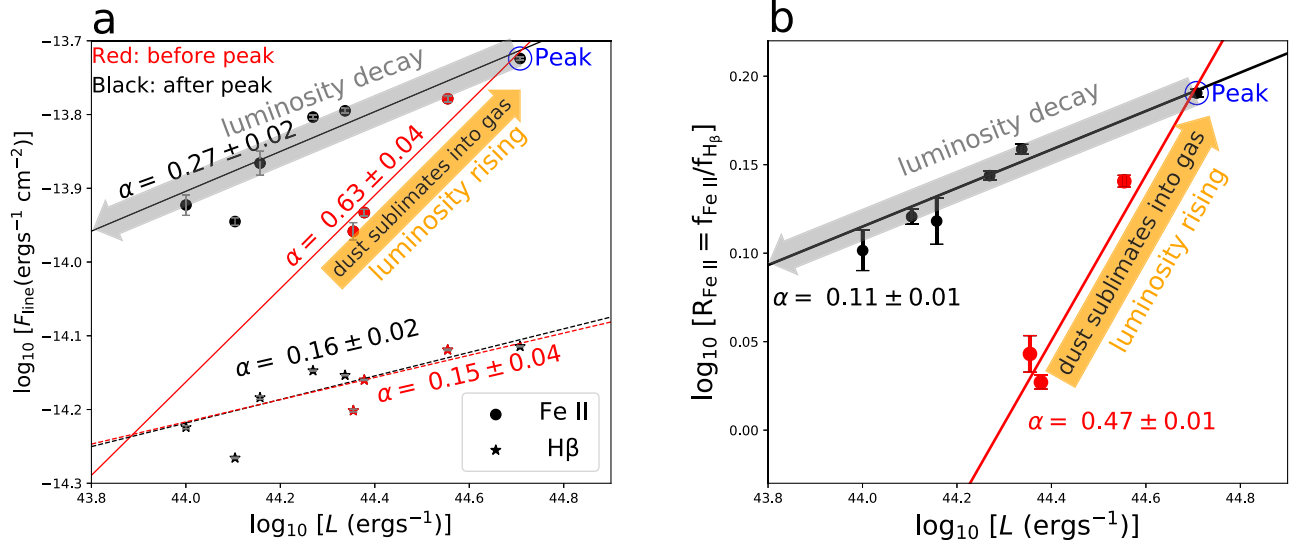


Figure 3. The hysteresis phenomenon of the Fe II and $R_{\text{Fe II}}$ line evolution in the TDE. Panel (a): the dots and stars are the Fe II and H β , respectively. The values of best-fitted α for each line are marked. The α in the luminosity rising phase is significantly greater than that in the decline phase. At the same luminosity, the Fe II emission in the decline phase is significantly greater than that in the rising phase. The evolutionary trajectory of Fe II forms a tilted “ Λ ” shape (i.e., a hysteresis effect), which indicates that the amount of Fe II-emitting gas in the decline phase is greater than that in the rising phase. Meanwhile, there is no significant difference for H β variation rate between the two phases. This result indicates that its dominant radiation region is likely closer than that of Fe II and is not dominated by the evaporated dust. Panel (b): similarly to Fe II, the evolutionary trajectory of $R_{\text{Fe II}}$ also shows a hysteresis effect.

grains, which emit very similarly to a blackbody. Replacing R_{sub} with the corresponding time lag $\tau_{\text{Fe II}} = \tau_{\text{sub}} = R_{\text{sub}}/c$, the AGN luminosity L_{bol} can be written as (Hönig et al. 2017):

$$L_{\text{bol}} = k\tau_{\text{Fe II}}^2 c^2, \quad (3)$$

where k is a parameter absorbing T_{sub} , f_{abs} , and Q_{abs} ; p . A luminosity distance D_L independent of redshift is calculated as:

$$D_L = \sqrt{\frac{k}{4\pi F}} \tau_{\text{Fe II}} c, \quad (4)$$

where F is the flux of the optical continuum. The parameter k can be calibrated by another cosmic distance ladder or the spatially resolved near-IR interferometry for the inner radius of the torus (Hönig 2014). Combination with the size of the time lag and the angular diameter θ from the interferometry for the inner radius of the torus, the angular diameter distance can be determined as $D_A = \tau_{\text{Fe II}} c / \theta$. According to the relationship $D_L = D_A(1+z)^2$, the k can be determined as $k = 4\pi F(1+z)^4 / \theta^2$. The scatter of k is found to be about 0.13 dex in the lag–luminosity relation of a sample of 17 AGN (Koshida et al. 2014). The scatter of k reflects the actual object-to-object differences in hot-dust composition, geometry, and global distribution in a sample. The low scatter value implies the tighter relation between time lag and luminosity, and the simple physics of the inner radius of the torus.

4.2. Other Possible Origins of the Extraordinary Response of the Iron Emission

The observed Fe II is related not only to the central ionization continuum but also to the spatial distribution of the gas around the central black hole accretion disk. On the one hand, the central ionization continuum may be different before and after a TDE, even at the same measured optical luminosity. On the other hand, the spatial distribution of gases may be different

The hysteresis effect of Fe II evolution

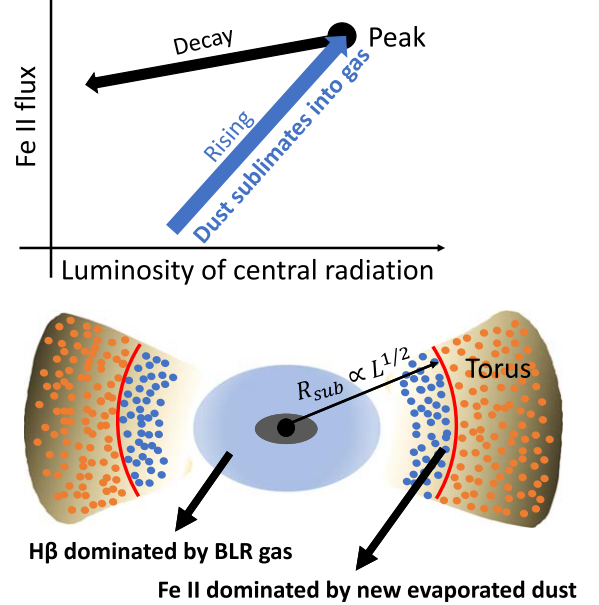


Figure 4. Schematic of Fe II originating from the evaporated dust at the inner surface of the torus in TDEs. As the central luminosity increases, the inner boundary of the dusty torus will recede to a larger radius. The metals released from the evaporated dust will give rise to the observed Fe II lines. The amount of evaporated dust reaches the maximum at the peak of central luminosity. As a result, at the same luminosity, the Fe II emission in the decline phase will be greater than that in the rising phase. The evolutionary trajectory of Fe II forms a tilted “ Λ ” shape (i.e., a hysteresis effect). Considering that the Fe II emission is dominated by the evaporated dust at the inner radius of the torus, which is related to the central luminosity, i.e., $R_{\text{sub}} \propto L^{1/2}$, the Fe II time lag can be adopted as a potential “standard candle” in cosmology.

before and after a TDE. For example, the unbound debris may fall back or the fast outflow (e.g., Hung et al. 2019) may emerge in a TDE. We will need more data to test these possibilities in the future. Anyway, the different power laws of

the Fe II response before and after a TDE are worth further study.

5. Conclusion


In this Letter, we present the response of Fe II emission in the PS1-10adi TDE, an AGN at $z = 0.203$. The time lag between optical continuum peak and Fe II or $R_{\text{Fe II}}$ strength peak is consistent with the torus inner radius. Furthermore, we find the Fe II variation rate in the luminosity rising phase to be significantly greater than that in the decline phase. At the same luminosity, the Fe II emission in the decline phase is significantly greater than that in the rising phase. The evolutionary trajectory of Fe II and $R_{\text{Fe II}}$ show an intriguing hysteresis effect. This result strongly suggests that the Fe II emission is boosted by the evaporated dust at the scale of the torus' inner radius. Our results reveal at least two applications of the Fe II emission in the TDEs:

1. The indicator of Eddington ratio: we propose that the dust sublimation of the AGN torus accompanied with the central outburst plays a key role in the rapid increase of Fe II strength. The irons, which were originally locked in the dust grains, get a chance to enter into the gas phase due to the sublimation and boost the Fe II emission. The Fe II strength is thus directly dependent on the amount of evaporated dust, which increases with the central luminosity. However, the evaporated region might contribute much less to the $H\beta$ emission. This indicates the $H\beta$ prefers a significantly smaller emission radius. As a result, this scenario naturally explains the physical mechanism leading to the increase of Fe II strength with Eddington ratio.
2. The potential cosmological application: since the Fe II emission is dominated by the evaporated dust at the inner radius of the torus, which is related to the central luminosity, i.e., $R_{\text{sub}} \propto L^{1/2}$, the Fe II time lag relative to the central luminosity can be adopted as a potential "standard candle" in cosmology. In the future, we can follow-up on the optical spectrum observation after the optical burst of a TDE. We are entering an age of accelerating development of time domain astronomy with the advent of a batch of dedicated modern surveys (e.g., ZTF, LSST, and WFST; Lou et al. 2016). For instance, the predicted TDE number found by LSST every year can be in the range of a few thousand (e.g., Thorp et al. 2019; Bricman & Gomboc 2020), which could include hundreds of events in AGN assuming an AGN fraction of 10%. Timely spectroscopic observations of these AGNs are highly encouraged to capture the peak of Fe II emission. The notion of Fe II "cosmological standards" can be soon tested and applied based on large sample studies.

We thank the anonymous referee for valuable comments and constructive suggestions. We also thank Dr. Erkki Kankare for providing us with the optical spectra data of PS1-10adi. Z.-C. H. is supported by NSFC-11903031 and USTC Research Funds of the Double First-Class Initiative YD 3440002001. N.J. is supported by NSFC-12073025. G.-L.L. acknowledges

the grant from the National Natural Science Foundation of China (No. 11673020 and No. 11421303) and the Ministry of Science and Technology of China (National Key Program for Science and Technology Research and Development, No. 2016YFA0400700). H.-X.G. acknowledges NSF grant AST-1907290. Y.-H.X. is partially supported by the NSFC-U1731127. This work is also supported by NSFC (11833007, 11973002, 11822301).

ORCID iDs

Zhicheng He  <https://orcid.org/0000-0003-3667-1060>
 Ning Jiang  <https://orcid.org/0000-0002-7152-3621>
 Tinggui Wang  <https://orcid.org/0000-0002-1517-6792>
 Guilin Liu  <https://orcid.org/0000-0003-2390-7927>
 Mouyuan Sun  <https://orcid.org/0000-0002-0771-2153>
 Hengxiao Guo  <https://orcid.org/0000-0001-8416-7059>
 Xinwen Shu  <https://orcid.org/0000-0002-7020-4290>
 Zhixiong Liang  <https://orcid.org/0000-0002-2384-3436>

References

- Bañados, E., Venemans, B. P., Mazzucchelli, C., et al. 2018, *Natur*, 553, 473
 Barth, A. J., Pancoast, A., Bennert, V. N., et al. 2013, *ApJ*, 769, 128
 Blanchard, P., Nicholl, M., Berger, E., et al. 2017, *ApJ*, 843, 106
 Boroson, T. A. 2002, *ApJ*, 565, 78
 Boroson, T. A., & Green, R. F. 1992, *ApJS*, 80, 109
 Bricman, K., & Gomboc, A. 2020, *ApJ*, 890, 73
 Czerny, B., Hryniewicz, K., Maity, I., et al. 2013, *A&A*, 556, A97
 Dong, X.-B., Wang, J.-G., Ho, L. C., et al. 2011, *ApJ*, 736, 86
 Drake, A., Djorgovski, S., Mahabal, A., et al. 2011, *ApJ*, 735, 106
 Ferland, G. J., Hu, C., Wang, J.-M., et al. 2009, *ApJL*, 707, L82
 Hoenig, S. F., & Kishimoto, M. 2011, *A&A*, 534, A121
 Hönig, S., Watson, D., Kishimoto, M., et al. 2017, *MNRAS*, 464, 1693
 Hönig, S. F. 2014, *ApJL*, 784, L4
 Hung, T., Cenko, S., Roth, N., et al. 2019, *ApJ*, 879, 119
 Jiang, N., Wang, T., Mou, G., et al. 2019, *ApJ*, 871, 15
 Jiang, N., Wang, T., Yan, L., et al. 2017, *ApJ*, 850, 63
 Kankare, E., Kotak, R., Mattila, S., et al. 2017, *NatAs*, 1, 865
 Kishimoto, M., Hönig, S. F., Antonucci, R., et al. 2013, *ApJL*, 775, L36
 Kishimoto, M., Hönig, S. F., Beckert, T., & Weigelt, G. 2007, *A&A*, 476, 713
 Kokubo, M., & Minezaki, T. 2020, *MNRAS*, 491, 4615
 Koshida, S., Minezaki, T., Yoshii, Y., et al. 2014, *ApJ*, 788, 159
 Koshida, S., Yoshii, Y., Kobayashi, Y., et al. 2009, *ApJL*, 700, L109
 Lawrence, A., Elvis, M., Wilkes, B. J., McHardy, I., & Brandt, N. 1997, *MNRAS*, 285, 879
 Lou, Z., Liang, M., Yao, D., et al. 2016, Proc. SPIE, 10154, 101542A
 Marziani, P., Sulentic, J., Zwitter, T., Dultzin-Hacyan, D., & Calvani, M. 2001, *ApJ*, 558, 553
 Mortlock, D. J., Warren, S. J., Venemans, B. P., et al. 2011, *Natur*, 474, 616
 Namekata, D., & Umemura, M. 2016, *MNRAS*, 460, 980
 Panda, S., Czerny, B., Adhikari, T. P., et al. 2018, *ApJ*, 866, 115
 Panda, S., Marziani, P., & Czerny, B. 2019, *ApJ*, 882, 79
 Rees, M. J. 1988, *Natur*, 333, 523
 Risaliti, G., & Lusso, E. 2019, *NatAs*, 3, 272
 Shen, Y., & Ho, L. C. 2014, *Natur*, 513, 210
 Shields, G. A., Ludwig, R. R., & Salvander, S. 2010, *ApJ*, 721, 1835
 Sun, M., Xue, Y., Wang, J., Cai, Z., & Guo, H. 2018, *ApJ*, 866, 74
 Thorp, S., Chadwick, E., & Sesana, A. 2019, *MNRAS*, 488, 4042
 Trakhtenbrot, B., Arcavi, I., Ricci, C., et al. 2019, *NatAs*, 3, 242
 Wang, J.-M., Songsheng, Y.-Y., Li, Y.-R., Du, P., & Zhang, Z.-X. 2020, *NatAs*, 4, 517
 Wang, T., Brinkmann, W., & Bergeron, J. 1996, *A&A*, 309, 81
 Watson, D., Denney, K., Vestergaard, M., & Davis, T. M. 2011, *ApJL*, 740, L49
 Yang, J., Wang, F., Fan, X., et al. 2020, *ApJL*, 897, L14